Applied Surface Science 493 (2019) 691–702

Contents lists available at ScienceDirect

Applied Surface Science

journal homepage: www.elsevier.com/locate/apsusc

Full length article

Epitaxial growth of cobalt doped TiO_2 thin films on $LaAlO_3$(100) substrate by molecular beam epitaxy and their opto-magnetic based applications

Swaleha Naseem[a], Igor V. Pinchuk[b], Yunqiu Kelly Luo[b], Roland K. Kawakami[b], Shakeel Khan[a], Shahid Husain[c], Wasi Khan[c,*]

[a] Department of Applied Physics, Z.H. College of Engineering & Technology, Aligarh Muslim University, Aligarh, 202 002, India
[b] Department of Physics, The Ohio State University, Columbus, OH 43210, USA
[c] Department of Physics, Aligarh Muslim University, Aligarh, 202 002, India

ARTICLE INFO

Keywords:
Anatase TiO_2
Molecular beam epitaxy
XPS
Room temperature ferromagnetism
Photocatalytic
Photoconductivity

ABSTRACT

In this work, we report the growth process of pristine and cobalt (2%, 4%, 6% and 8%) doped TiO_2 thin films on $LaAlO_3$(100) substrate by molecular beam epitaxy (MBE) technique. The microstructural, magnetic, optical, photoconductivity and photocatalytic activity of the films were explored. Reflection high-energy electron diffraction (RHEED) confirms successful growth of single phase anatase TiO_2 thin film and effects of cobalt (Co) doping on crystal phase depending on the growth conditions and correlating changes in their physical properties. X-ray diffraction and X-ray photoelectron spectroscopy (XPS) establish highly pure crystalline nature and oxidation state of the elements. Magnetic measurements show room temperature ferromagnetism in all the thin films and suggest that growth conditions, oxygen vacancies and bound magnetic polaron (BMP) model account for the magnetic properties. The optical properties exhibit a red shift response associated with narrowing bandgap that influence photocatalytic activity. The 8% cobalt doped TiO_2 film has shown 91% degradation with methylene blue and 88% degradation with Azo dye in 70 min under visible light irradiation exhibiting excellent photocatalytic performance. The photoconductivity measurements have confirmed photosensitive nature of TiO_2 and 8% Co doped TiO_2. Therefore, these opto-magnetic properties can be tuned for the applicability of future spintronic and optical devices.

1. Introduction

Diluted magnetic semiconductors (DMS) are promising materials having small percentage doping of transition metal ions with unpaired '*d*' electrons in the semiconducting host material. They have attracted attention because of their potential applications in future spintronic devices like spin transistors, spin logic and storage devices [1–4]. In this novel technology, both spin and charge are involved to store, transport and process information, however, it ensures improvement in performance by increasing both speed and storage capacity in classical microelectronic devices [5]. In recent years, intensive attention has been given by researchers, after the remarkable discovery by Matsumato et al. [6] of high T_c ferromagnetism in Co-doped TiO_2. Similarly, Dietl et al. [7] predicted theoretically and experimentally room temperature ferromagnetism (RTFM) in Mn doped ZnO and in other transition metal (TM) doped wide band gap semiconductors such as SnO_2, TiO_2 and HfO_2. Yang et al. [8] observed the presence of RTFM in C doped TiO_2 in both anatase and rutile structures whereas Coey et al. [9] reported magnetism (known as d^0 magnetism) in HfO_2 thin films grown on sapphire and silicon substrates which encouraged explaining the real origin of magnetism. Among these DMS materials, Co doped TiO_2 came out to be a capable candidate owing to its excellent properties like stability, transparency, high n type carrier mobility and low cost.

Moreover, TiO_2 has attracted a lot of attention over the last two decades on the basis of its wide range of applications such as photocatalysis, photovoltaic cells, gas sensors, transparent conducting oxides and dye sensitized solar cells [10–13]. It has polymorphic crystal structures namely; anatase, brookite and rutile, where anatase and brookite are metastable phases that convert to thermally stable rutile phase on heat treatment at 600 to 1200 °C. Among these, anatase phase shows better photocatalytic activity in comparison to other phases due to the formation of high hydroxylate surface in this phase that is responsible for photocatalytic reaction [14]. Energy crisis and water pollution are two major issues prevailing these years, however for solving these issues, anatase TiO_2 can be utilized in optical degradation of organic compounds and purification of water and air. In 1972,

* Corresponding author.
E-mail address: wasi.ph@amu.ac.in (W. Khan).

https://doi.org/10.1016/j.apsusc.2019.07.017
Received 23 May 2019; Accepted 2 July 2019
Available online 03 July 2019

Fujishima and Honda [13] reported photocatalysis of water. Since then, anatase TiO_2 has been studied for the degradation of organic pollutants and dye sensitized solar cells. Photocatalytic reactions like hydrogen generation, decomposition of organic substances and photo-induced hydrophilicity takes place on the contact surface. Therefore, thin films are suitable for photocatalytic and solar cell applications. Numerous studies have been devoted to develop visible light driven TiO_2 based photocatalyst by doping transition metal and non-metal impurities [15–17]. Introduction of impurities such as substitutional or interstitial metal ions or anion in crystalline titania, creates impurity states. The newly created interband energy states result in a decrease of the photo threshold energy of TiO_2. However, it is still challenging to synthesize high efficient TiO_2 based photocatalysts. It would be beneficial if this metal oxide semiconductor could be photosensitized in visible light. The photoconductivity measurements involve the interpretation of photosensitivity, photo generation, recombination and trapping [18,19]. Earlier, it was reported that substitution of transition metal ions to anatase TiO_2 lattice does not boost the photo-oxidative activity but in many cases it decreases too [20].

There are several reports on the growth of TiO_2 films on various substrates like Al_2O_3, $LaAlO_3$, $SrTiO_3$, $BaTiO_3$ and GaN that depend on conditions of deposition and choice of substrate for specific anatase, rutile or mixed phases of TiO_2 [21–25]. Appropriate choice of substrate like $LaAlO_3$ or $SrTiO_3$ enables to grow anatase phase of TiO_2 with high crystallinity. In earlier reported work, films were grown by various techniques like pulse laser deposition (PLD), chemical vapour deposition (CVD), sputtering and oxygen plasma assisted molecular beam epitaxy (OPA-MBE). Out of these, molecular beam epitaxy (MBE) technique differs in thermodynamics and kinetics from other techniques and can produce high quality crystalline films of TiO_2 on $LaAlO_3$(LAO), $SrTiO_3$(STO) and GaN substrates which make an impact on film properties [26]. Films grown from PLD and OPA-MBE on $SrTiO_3$ (001) and $LaAlO_3$(001) have resulted in different magnetic properties for the two different growth methods. Researchers have confirmed that ferromagnetism is an effective combination of epitaxial structure that is emerging from interface of substrate and epitaxial thin film [27]. Shao et al. [22] have reported that the high growth rate in MBE is responsible for the nucleation of rutile phase of nanocrystals when TiO_2 is grown on LAO substrates. Therefore, it is observed that for anatase phase of TiO_2, slow growth rate is preferred for the deposition of the film on LAO (100) by MBE. In this study, we have grown anatase TiO_2 films on $LaAlO_3$ (100) substrate using molecular oxygen (O_2) MBE system equipped with high temperature effusion cells filled with titanium, cobalt and molecular oxygen as a source. In this work, slow growth rate has been preferred for the growth of pristine and Co (2%, 4%, 6% and 8%) doped anatase phase TiO_2 thin films of 20 nm thickness. We have analysed structural, magnetic influence, photocatalytic activity and photoconductivity of the prepared samples.

2. Materials and characterization

Growth of pristine and cobalt doped (2%, 4%, 6% and 8%) anatase phase TiO_2 thin films of chemical formula $Ti_{1-x}Co_xO_2$ ($0 \leq x \leq 0.08$) were grown in a MBE system equipped with in situ reflection high-energy electron diffraction (RHEED). Initially the $LaAlO_3$(100) substrates were ultrasonically treated with isopropanol, deionized water, and dried under flow of dry nitrogen gas. Prior to growth, the $LaAlO_3$(100) substrates were annealed at 700 °C for 1 h. For growth of anatase phase TiO_2, we have utilized a Ti electron-beam evaporator and molecular oxygen introduced by a sapphire-sealed leak valve. For cobalt doping, elemental Co from an effusion cell was used. The Ti and Co growth rates were measured by a quartz deposition monitor, and the partial pressure of molecular oxygen was estimated to be a large fraction of the overall chamber pressure; for a typical Ti growth rate of 0.42 Å/min, the chamber pressure was 533.28×10^{-9} Pa, while the typical chamber pressure after introducing molecular oxygen was $\sim 399.96 \times 10^{-7}$ Pa. Initially, a 2 nm TiO_2 buffer layer was grown on the $LaAlO_3$(100) by depositing Ti with molecular oxygen dosing ($\sim 399.96 \times 10^{-7}$ Pa) and sample temperature of 600 °C. For the pure TiO_2 samples, we subsequently deposited 20 nm TiO_2 under the same conditions. For cobalt-doped TiO_2 samples, the 20 nm thin films were grown by co-evaporating Co and Ti onto the TiO_2 buffer layer under similar conditions (600 °C, $\sim 399.96 \times 10^{-7}$ Pa). The doping level of Co was determined by measuring the relative atomic fluxes from the Co and Ti sources. Growth of the film was monitored by in situ RHEED at the applied voltage of 15 kV.

Our investigation consists of material synthesis by MBE, structural characterization by in situ RHEED, tapping mode atomic force microscopy (AFM) in a Bruker Icon 3 system, X-ray diffraction (XRD) in a Bruker D8 Discover system equipped with Cu-K_α $\lambda = 1.54$ Å wavelength X-ray source. The surface compositions of the samples and binding energies were determined by the X-ray photoelectron spectroscopy (XPS, Perkin-Elmer PHI 5600, Waltham, MA, USA). Magnetic properties at room temperature were studied by vibrating sample magnetometer (VSM), and optical properties using Perkin Elmer Spectrophotometer in visible region (300–800 nm) of the spectrum. Photoconductivity mapping of the prepared samples was studied using a tunable laser source (Fianium Supercontinuum WhiteLase and LLTF). The photocatalytic activity of prepared samples was studied by the degradation of two different organic dyes namely methylene blue (MB) and azo dyes in aqueous solution under visible light illumination. In a typical measurement, the solutions of dyes in desired concentration were prepared in deionized water then catalysts were kept in the MB and Azo solutions of initial concentration of 20 µg/ml in a beaker of 100 ml distilled water followed by magnetic stirring for 30 min in dark to attain adsorption equilibrium before the illumination under visible light source of 400 W sodium lamp. After that samples were illuminated and at the fixed interval (up to 70 min), 5 ml solution was analysed using UV–visible spectrophotometer. The photocatalytic degradation of the dyes was determined using the following equation:

$$\text{Photodegradation (\%)} = \frac{C_0 - C}{C_0} \times 100\%$$

where C_o is the initial concentration of dye before photodegradation and C gives the final concentration after the different time intervals.

3. Results and discussion

3.1. Structural analysis

Fig. 1(a) shows the RHEED pattern of substrate $LaAlO_3$(100) after annealing at 700 °C temperature. RHEED gives information of the surface structure of the film indicating in-plane crystallinity from the diffraction of high energy electrons. Significantly, it is possible to monitor the atomic layer-by-atomic growth of epitaxial films [28]. The RHEED pattern (Fig. 1(a)) shows the bright spots indicating that the substrate is atomically smooth. Initially, we have started the deposition of 2 nm buffer layer and then further continued the growth to get the anatase TiO_2 film of thickness 20 nm. The brightness of the RHEED pattern decreases as the deposition starts and then pattern changes to streaky as shown in Fig. 1. In order to understand the surface structure and growth mechanism of the film, it is important to monitor the RHEED patterns. We have observed that as the Co doping in TiO_2 increases from 2% to 8%, the streaky pattern changes to a spotty pattern. This change in RHEED indicates the island nucleation due to transition of growth mechanism during film deposition as Co ions get agglomerated on the substrate. For (100)-oriented anatase TiO_2 and with Co doped TiO_2 thin films, the RHEED patterns are shown in Fig. 1(b-f). The streaky behaviour shown in the beginning indicates atomic layer-by-layer growth. Later on, the streaky pattern becomes dim and we observe a noticeable change in RHEED as the growth time reaches about 2 h. Moreover, the pattern changes to a bright spot ring-like pattern with the increase in

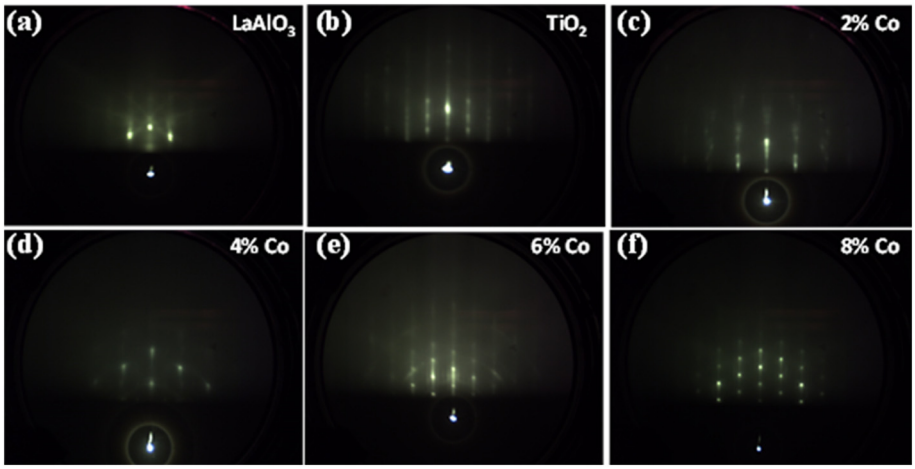

Fig. 1. RHEED patterns of (a) post annealed $LaAlO_3$(100) substrate at 700 °C, and (b–f) 0%, 2%, 4%, 6%, and 8% Co doped TiO_2 films of thickness 20 nm grown at 600 °C on $LAlO_3$(100) substrate.

doping level of cobalt that may be correlated with the incorporation of Co ions in TiO_2 host lattice leading to three dimensional growth or rough surface film [2]. The XRD scans for pristine and Co (2%, 4%, 6% and 8%) doped TiO_2 films on $LaAlO_3$ (100) substrate are shown in Fig. 2 that predict the anatase phase of the films. The sharp (004) peak of the films along with (100), (200) and (300) peaks of the substrate attributes to the successful epitaxial growth by MBE, which minimises the impurity incorporation. Distinctly, no other diffraction peak was observed, indicating single phase highly crystalline anatase TiO_2 thin films [29]. Moreover, no extra peak of any impurity is observed, suggesting the absence of clusters of Co or another phase of TiO_2. However, we have also noticed a decrease in intensity of diffracted peaks on substitution of Co ions that signify decrease in crystallinity due to formation of oxygen vacancies or crystal defects in order to neutralize the charge imbalance created in the titania lattice. The AFM images (2D) presented in Fig. 3 show the pristine, 4% and 8% Co doped TiO_2 thin film surface smoothness. From the images, it is clear that smoothness of the film decreases with the increase in doping percentage of cobalt in TiO_2 matrix. The *rms* roughness of the films is found to increase from 2.37 nm to 4.83 nm from pristine to 8% cobalt doped TiO_2 films on the scale of 1 μm. These results are in the correlation of RHEED pattern of the films. In addition, there is a wide range of particle distribution that is why atoms get displaced from underlying atoms and hence smoothness decreases.

3.1.1. X-ray photoelectron spectroscopy (XPS)

The X-ray photoelectron spectroscopy (XPS) is a sensitive tool to examine oxidation states of the constituent elements, chemical composition and valence state of materials. Shirley algorithm is implemented to the background core level spectra and non-linear curve fitting procedure is used to resolve the distinct elemental composition of undoped and Co doped TiO_2 thin films. The wide XPS spectra of undoped and 4% Co doped TiO_2 thin films are shown in Fig. 4(a). Core level high resolution spectra of Ti2p and O1s of undoped and 4% Co doped TiO_2 thin films are shown in Fig. 4(b-e). The presence of Ti^{4+} is clearly shown in the XPS spectra of Ti2p where two characteristic peaks at 462.63 eV ($2p_{1/2}$) and 456.92 eV ($2p_{3/2}$) are observed that may be originated from the spin orbit splitting. The binding energy difference, $\Delta = Ti2p_{1/2} - Ti2p_{3/2} = 5.71$ eV is found in good agreement with earlier reported values [30,31]. A shoulder peak at 457.80 eV corresponds to Ti^{3+} ($Ti2p_{1/2}$) of Ti_2O_3 that is found to be significantly lower intensity in the doped thin film sample. The slight binding energy shift and decrease in the intensity of shoulder peak further signifies decrease in the band gap with Co substitution in TiO_2 matrix [32]. A broad O1s peak observed at 528 eV for undoped TiO_2 thin film suggests the structural oxygen peak and confirms the lattice oxygen associated with TiO_2. The second peak at higher binding energy nearly 530.30 eV is due to chemically adsorbed oxygen and non-lattice oxygen [33]. However, a peak around 528.52 eV is possibly due to creation of oxygen vacancies at the cost of removal of oxygen atoms from TiO_2 lattice due to charge neutrality requirements as Ti^{4+}/Ti^{3+} is replaced by Co^{2+}. The slight shift in O1s peak could be due to difference in the oxygen vacancies of the prepared samples. However, this formation of oxygen defects is responsible for the magnetic interactions associated with Co doped TiO_2 thin films.

The core level $Co2p_{3/2}$ peak for 4% Co doped TiO_2 thin film is shown in Fig. 4(f). High resolution $Co2p_{3/2}$ peak observed at 779.59 eV and a lower intensity peak at 795.16 eV is attributed to the $Co2p_{1/2}$. The binding energy difference, $\Delta = Co2p_{1/2} - Co2p_{3/2} = 15.6$ eV nearly matches with the standard CoO [30] having high spin divalent state of Co^{2+} whereas binding energy difference for low spin Co^{3+} is 15 eV [34]. Furthermore, confirmation of 2+ state of Co is attributed from the two strong shake up satellite peaks toward the higher binding energy states of Co2p core level peak [34]. XPS data have ruled out the presence of metallic Co, since in that case difference Δ is 15.05 eV [30]. Therefore, XRD and XPS data have been well correlated showing no evidence of metallic cobalt.

3.2. Magnetic studies

The field dependent magnetization (M-H) plots for as-grown pristine and cobalt doped TiO_2 films are shown in Fig. 5. The M-H loop indicates that all thin films are ferromagnetic at room temperature and have higher values of saturation magnetization (M_s) as compared to previously reported results. It can be easily observed from the hysteresis loop that the ferromagnetic behaviour increases for cobalt-doped TiO_2 thin films as compared to undoped film. The ferromagnetic behaviour in pristine TiO_2 is proposed to originate from oxygen vacancies. Table 1 shows the saturation magnetization (M_s), coercive field (H_c), remanent magnetization (M_r) and squareness (M_r/M_s) ratio of all the prepared thin films. In order to compare the different behaviour of Co (2%, 4%, 6%, 8%) doped TiO_2 thin films, the in-plane (ip) and out-of-plane (op) hysteresis measurements were carried out and their comparison is shown in Fig. 6. For thin film samples, magnetic anisotropy can be explained as the difference in magnetization along in-plane and out-of-plane directions. It depends on various factors like shape anisotropy, stress anisotropy and interface exchange anisotropy. The remanence to saturation magnetization (M_r/M_s) ratio for in-plane and out-of-plane directions varies for the doped samples. In addition, the coercive field (H_c) for the out- of-plane direction is larger than H_c for in-plane

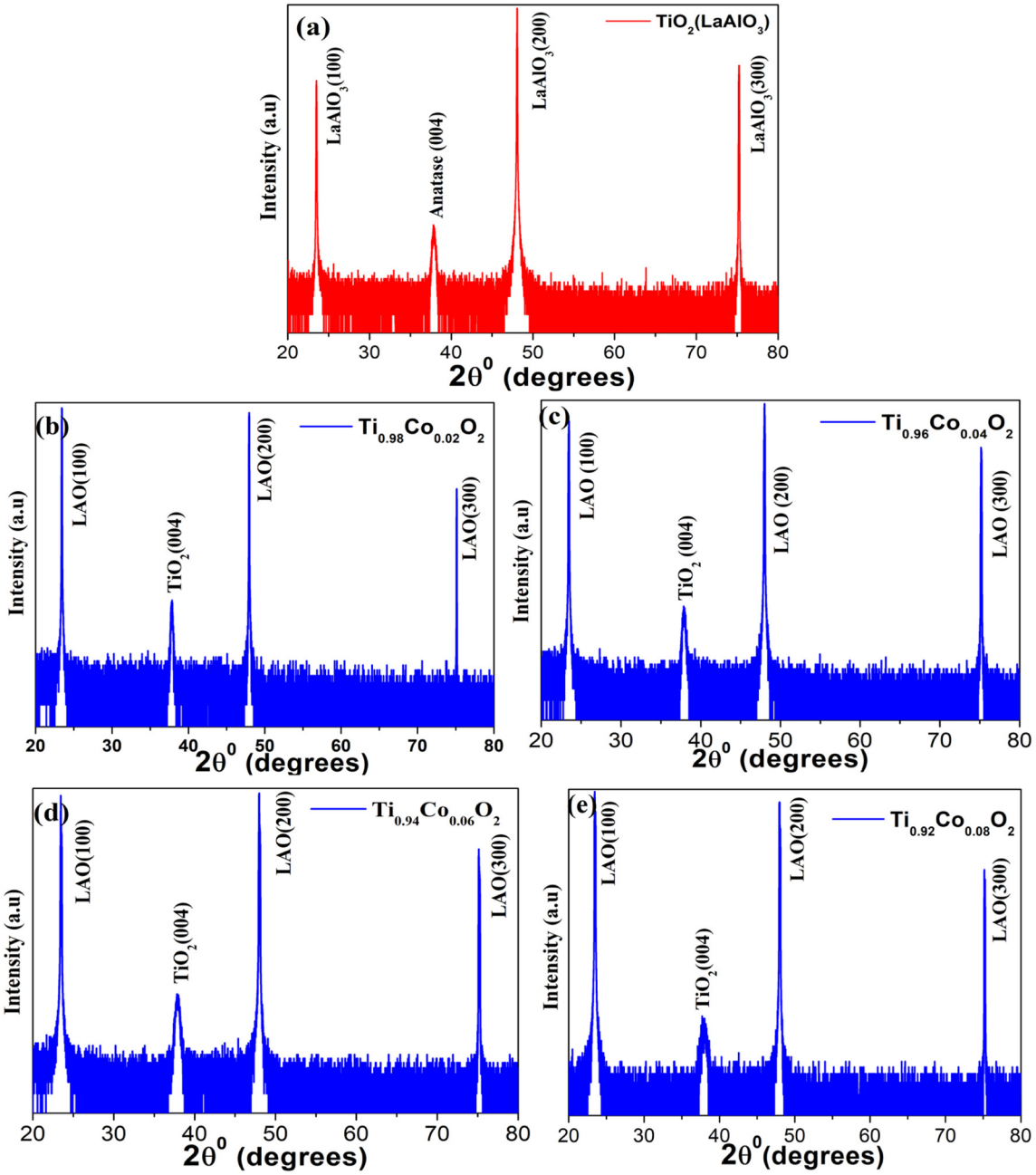

Fig. 2. XRD patterns of pristine and Co (2%, 4%, 6% and 8%) doped TiO_2 thin films on $LaAlO_3$(100) substrate.

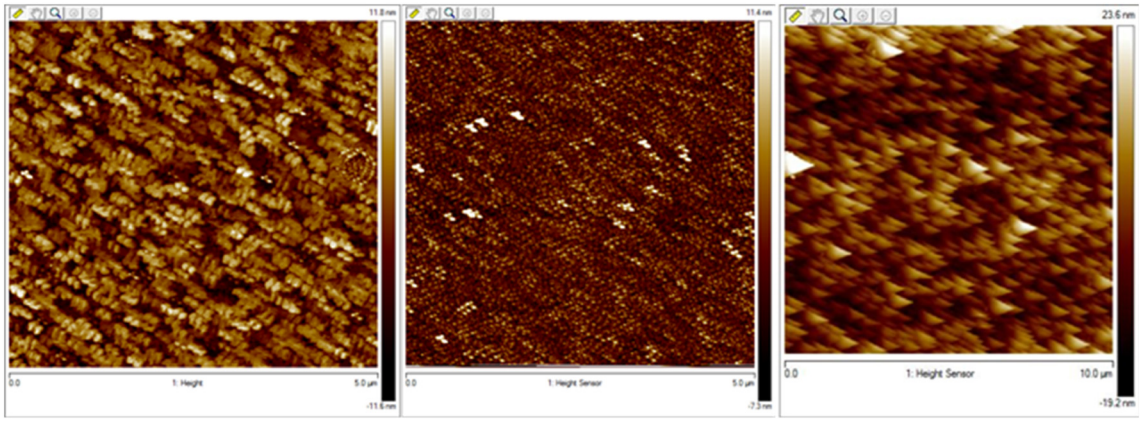

Fig. 3. 2D AFM images of pristine and Co (4% and 8%) doped TiO_2 thin films on $LaAlO_3$(100) substrate.

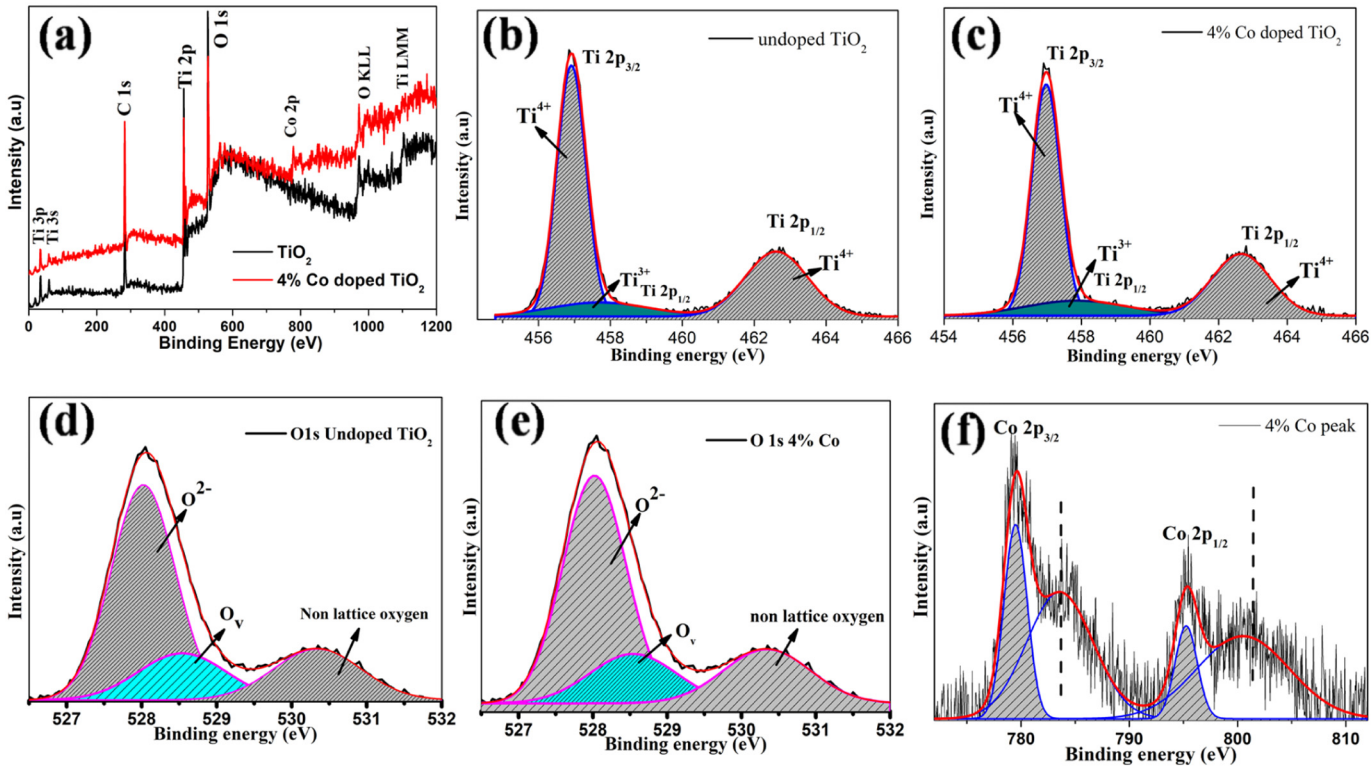

Fig. 4. (a) XPS survey spectra, (b,c) high resolution XPS spectra of Ti2p and (d,e) O1s peaks for undoped and 4% Co doped TiO_2; and (f) high resolution XPS spectra of Co2p peaks for 4% Co doped TiO_2 thin film.

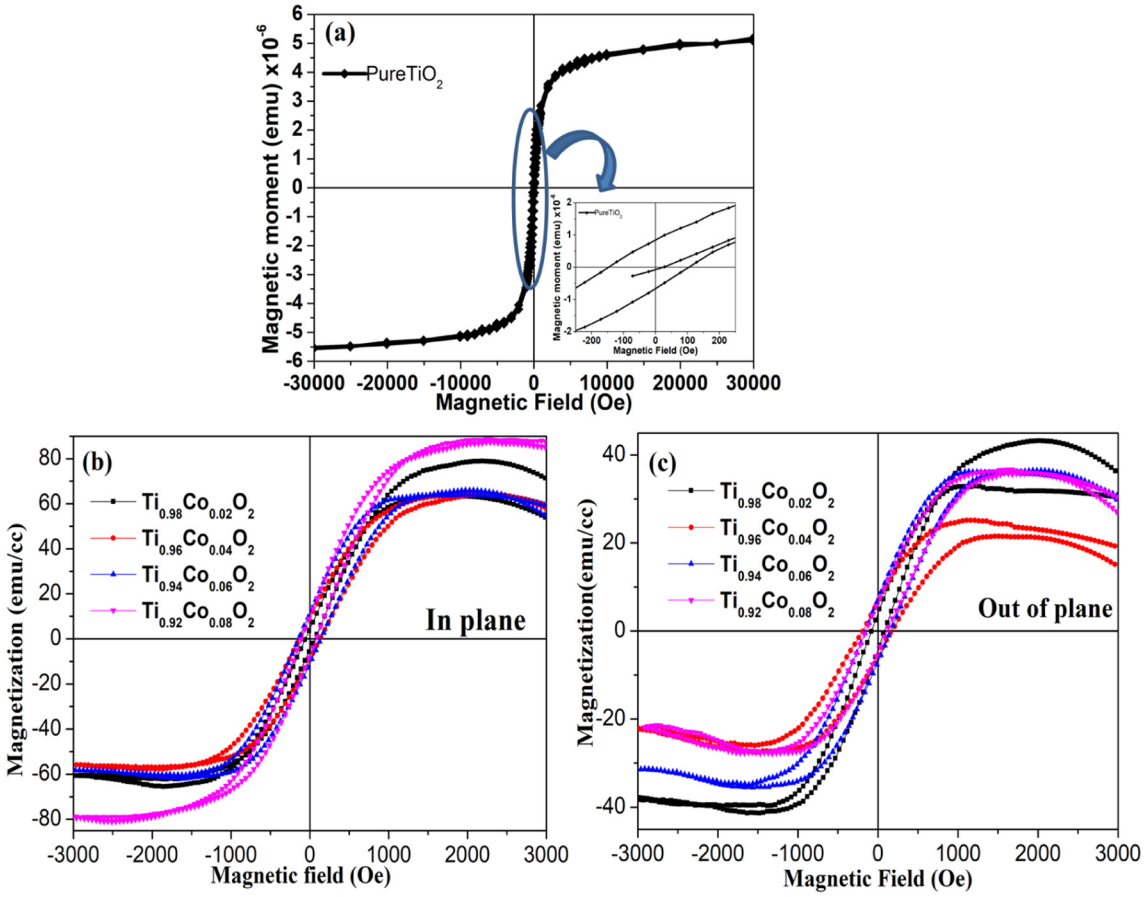

Fig. 5. Room temperature M-H hysteresis loops of ferromagnetic component for $Ti_{1-x}Co_xO_2$ ($0 \le x \le 0.08$) thin films on $LaAlO_3$(100) substrate when applied field is in plane and out of plane respectively.

Table 1
Room temperature magnetic parameters: coercivity (H_c), remanent magnetization (M_r), saturation magnetization (M_s), squareness (M_r/M_s), anisotropy constant (K) and magneton number (μ_B) for $Ti_{1-x}Co_xO_2$ ($0 \le x \le 0.08$) thin films.

Conc. (x)	In plane				Out of plane					
	H_c (Oe)	M_r (emu/cc)	M_s (emu/cc)	M_r/M_s $\times 10^{-3}$	H_c (Oe)	M_r (emu/cc)	M_s (emu/cc)	M_r/M_s $\times 10^{-3}$	K $\times 10^2$	μ_B $\times 10^{-2}$
$x = 0.2$	59.1	4.57	62.24	73	81.6	4.14	37.04	11	31.47	53.1
$x = 0.4$	131.4	8.84	60.79	145	179.9	6.245	24.08	259	45.12	34.5
$x = 0.6$	144.4	11.21	62.36	179	163.0	7.19	35.01	205	59.43	50.1
$x = 0.8$	96.4	5.60	83.46	67	135.3	5.875	31.67	185	44.64	45.4

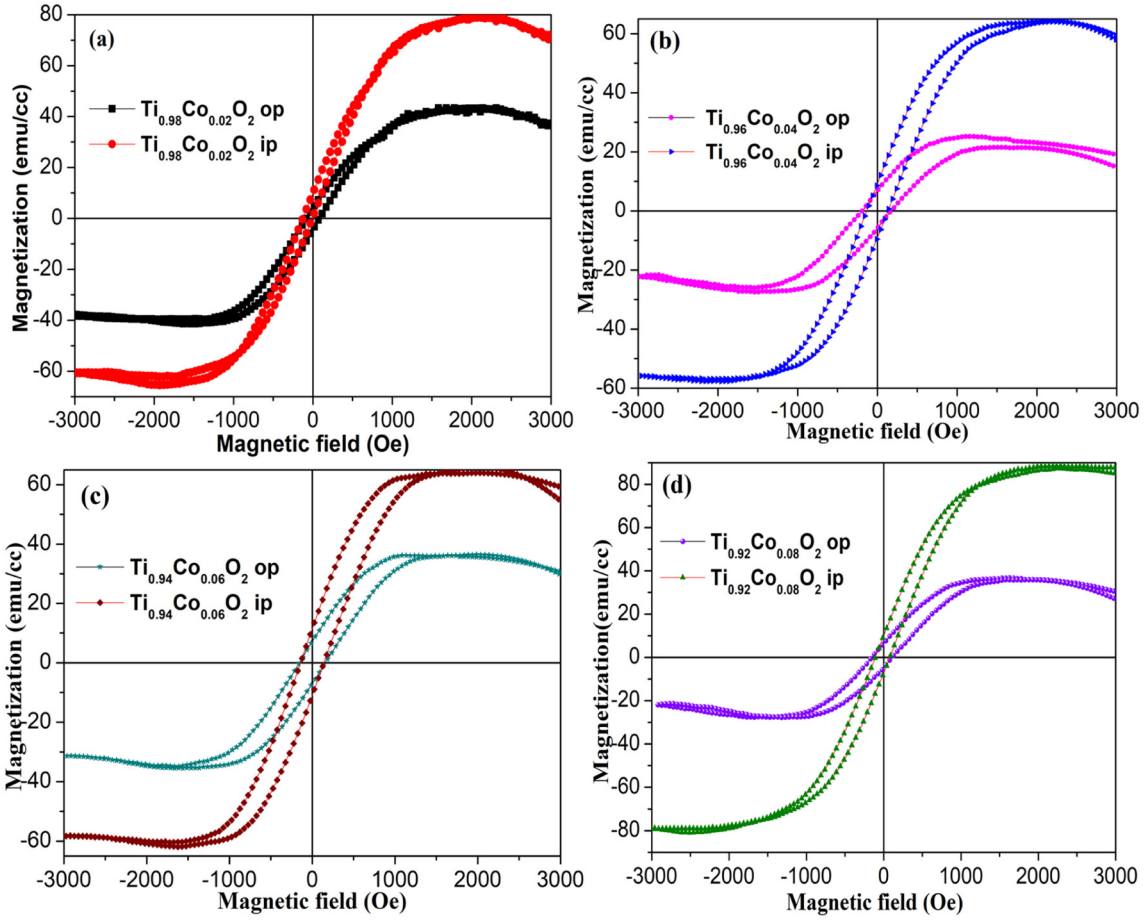

Fig. 6. Comparison of in-plane (ip) and out-of-plane (op) magnetic components for (a) 2%, (b) 4%, (c) 6%, and (d) 8% Co doped TiO_2 thin films.

direction, which signify that the spin state is more stable for the out-of-plane direction [35]. These observations indicate an out-of-plane easy axis. The anisotropy constant (K) for the easy axis samples has been calculated by the equation, $H_c = (0.96 \times K)/M_s$ and magneton number (μ_B) (saturation magnetization per formula unit in Bohr magneton) of the samples was calculated using equation [36], $\mu_B = (M.\ wt \times M_s)/5585$ and tabulated in Table 1. The origin of the ferromagnetism is not well understood and experimental results show varied behavior depending on synthesis techniques and growth conditions [37]. Despite one of the mechanisms proposed behind the RTFM in undoped TiO_2 film is based on the intrinsic oxygen vacancies that behave as donors resulting to n-type doping of material. Kim et al. [38] have explained that the oxygen vacancies play an important role for RTFM in pristine and transition metal doped TiO_2 thin films. Hong et al. [37] have performed experiments on thin films to investigate the role of oxygen vacancies on the ferromagnetic properties. Researchers reported that annealing of ferromagnetic TiO_2 thin film in an oxygen atmosphere for few hours to reduce oxygen vacancies leads to a substantial reduction of the magnetic moment. Hence, this gives evidence of the role and importance of oxygen vacancies in RTFM of TiO_2 films. However, the mechanism for generating ferromagnetism in the TiO_2 remain unclear as several theories were proposed including carrier-mediated Ruderman-Kittel-Kasuya-Yoshida (RKKY) and coupling of bound magnetic polarons (BMP) [5]. Theory applied for metallic systems having large number of delocalized electrons is RKKY whereas theory applied for semiconductors or insulators having localized electrons created due to oxygen vacancy defects and surrounding transition metal cations is BMP [39]. Presence of abundant oxygen vacancies or absence of magnetic impurity in our samples, supports an explanation of signatures of ferromagnetism in terms of the BMP model. In our growth process of samples at 600 °C, the high temperature favours phase transformation that increases the interfacial and structural defects leading to increase in number of oxygen vacancies. However, high temperature increases oxygen vacancy mobility with the increase in both concentration and

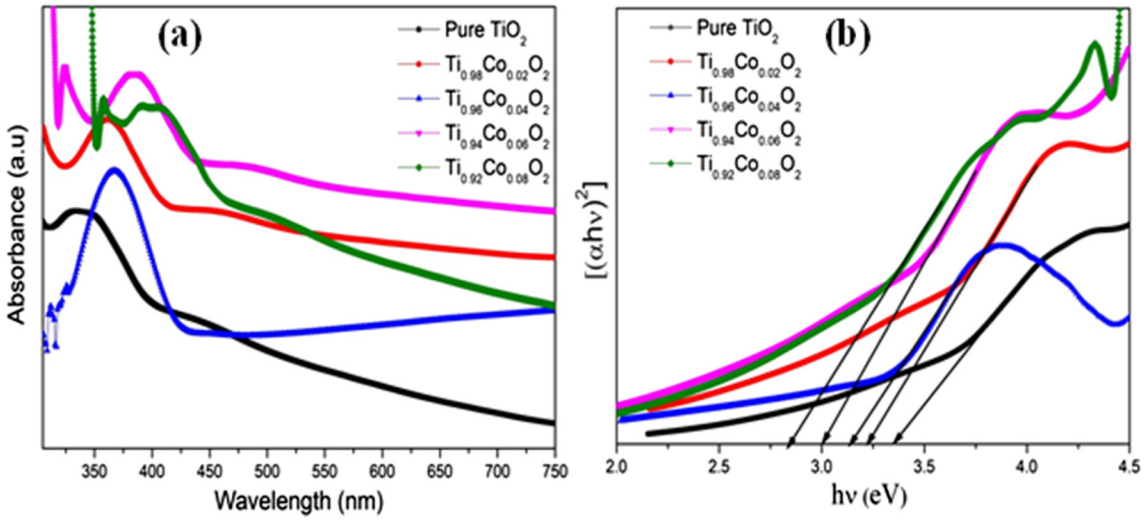

Fig. 7. (a) Absorbance spectra and (b) Tauc's plots for $Ti_{1-x}Co_xO_2$ ($0 \leq x \leq 0.08$) thin films on $LaAlO_3$(100) substrate.

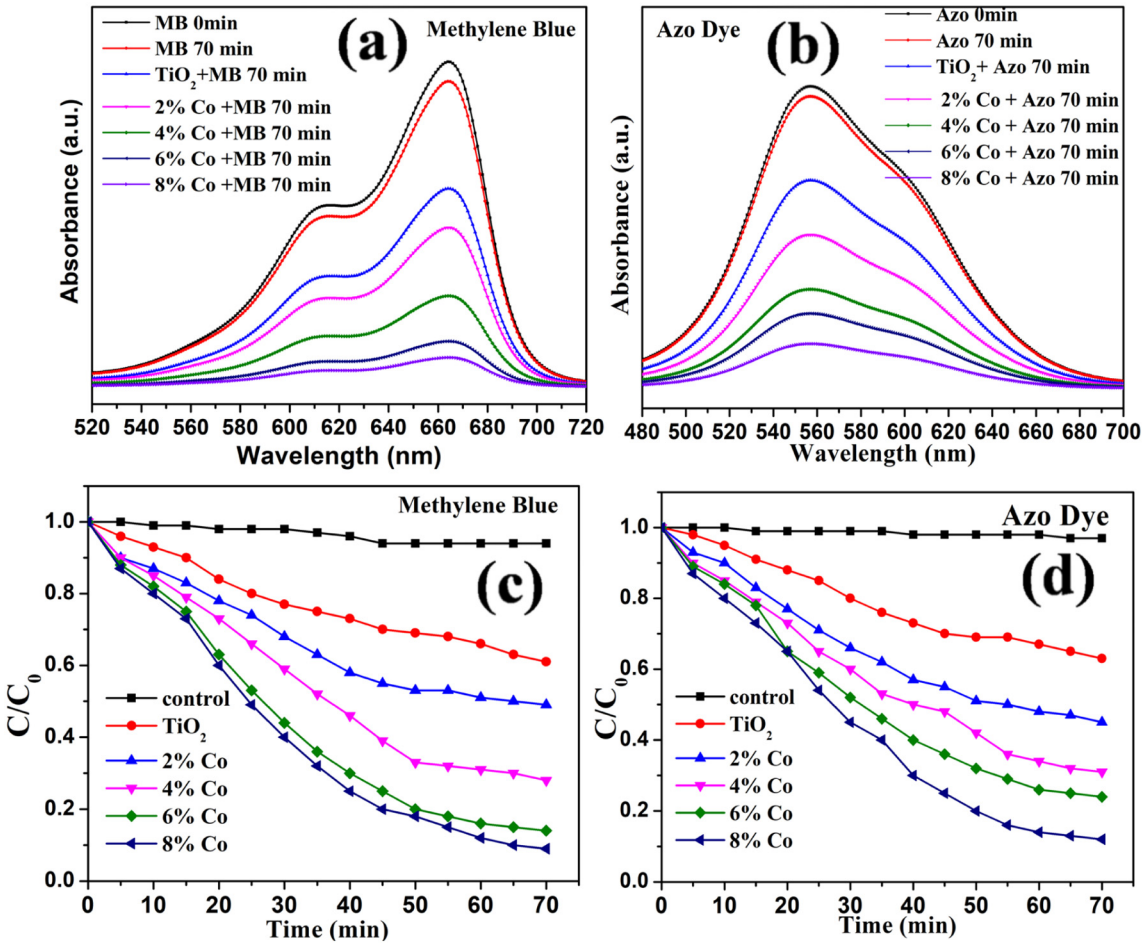

Fig. 8. (a,b) Absorbance spectra of methylene blue (MB) and azo dyes; (c,d) degradation of the same dyes in the presence of catalysts after 70 min duration. (For interpretation of the references to colour in this figure legend, the reader is referred to the web version of this article.)

diffusivity of defects in TiO_2 lattice, creating so called oxygen vacancies and defect clusters. Schwartz et al. [40] have explained that mechanism for ferromagnetic activation in oxide thin films is due to the formation of interface oxygen vacancies during the growth. Coey et al. [41] have explained how oxygen vacancies introduced at the interface of film/substrate could describe moment per cation which increases the spin value in transition metal doped TiO_2 thin film systems. When electrons which exist around cobalt ions get trapped in oxygen vacancies and defects, they form the BMP. In our samples, we have observed large order ferromagnetism at room temperature that can be attributed due to oxygen vacancies and structure defects present in the system. When the density of defects is significant to form hydrogen like orbitals (coupling of Co ions with donor electron) at random position forming a large magnetic cluster in the crystal lattice, this leads to long range

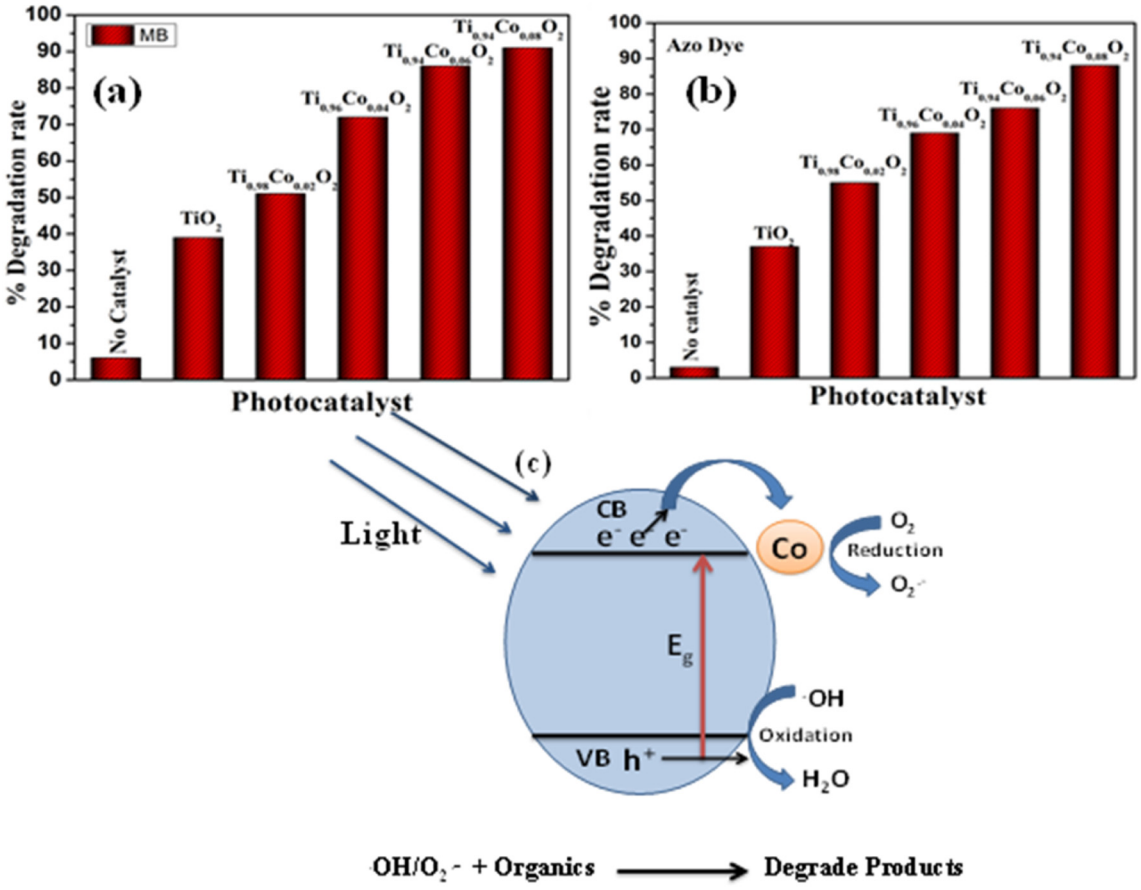

Fig. 9. (a,b) Percentage degradation of MB and azo dyes in presence of catalysts, **(c)** Possible photocatalytic mechanism.

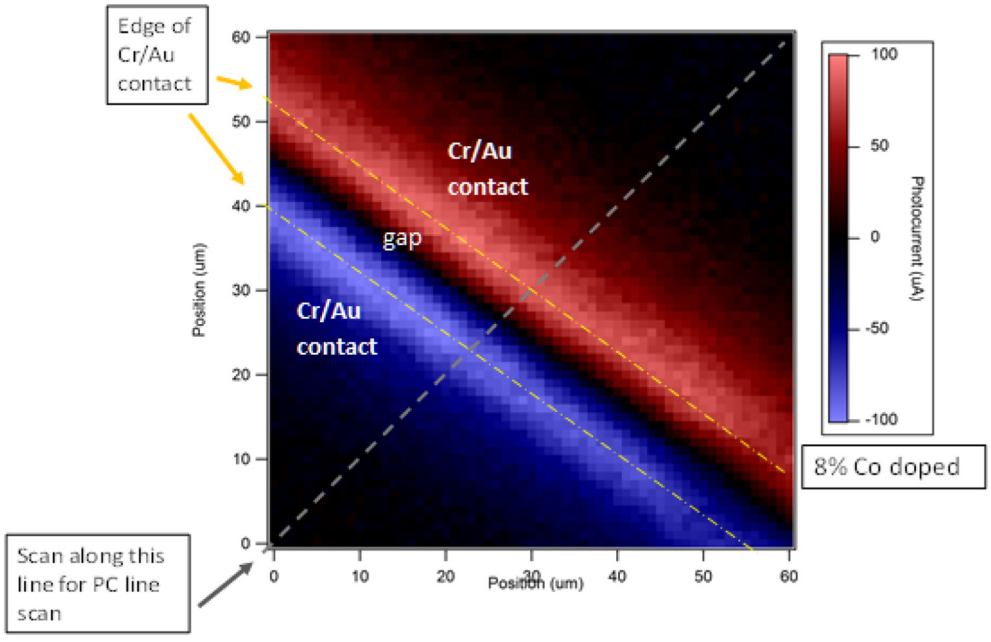

Fig. 10. Scanning photocurrent (PC) microscopy image for the 8% Co doped TiO_2 film.

ferromagnetic order [42,43].

3.3. Optical properties

UV–visible absorption spectroscopy is used to investigate the effect of impurity dopants on the optical properties of semiconducting nanostructures. A small percentage doping of transition metals ions is expected to make changes in the optical behaviour as compared to the host lattice. Absorption spectra were recorded in the wavelength region of 300–800 nm and shown in Fig. 7(a). This may be attributed to the

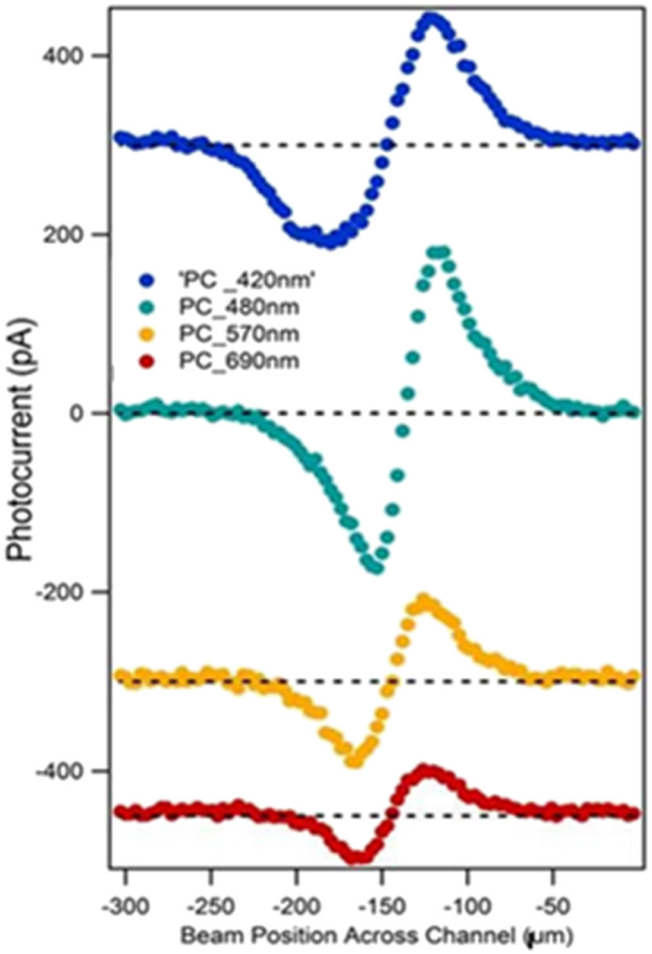

Fig. 11. PC signal magnitude versus beam position at different wavelength for 8% Co doped TiO_2 thin film. The data is taken along the line indicated in Fig. 10.

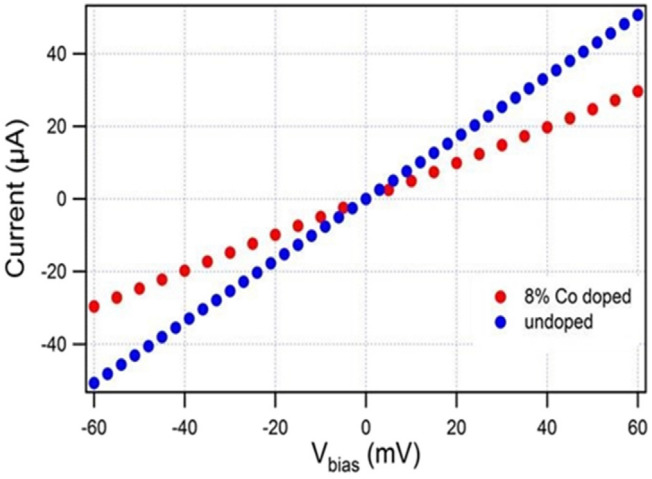

Fig. 12. Variation in current as a function of bias voltage for pristine and 8% Co doped TiO_2 films.

photo excitation of electrons originating from the valance band to the conduction band. A red shift is observed in the absorption spectra with the incorporation of cobalt in TiO_2 host lattice, which is consistent with previous reports [44]. In the energy band spectrum, the top of the valence band corresponds to the O_{2p} whereas the bottom of the conduction band to the Ti_{3d} state. Absorption band at around 380 nm for

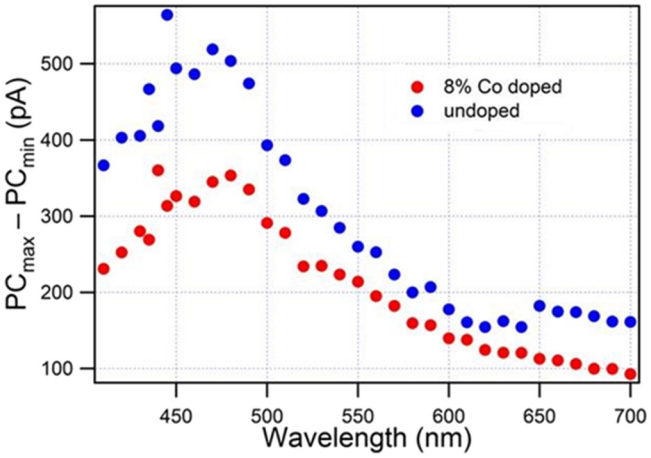

Fig. 13. PC line cut magnitude (PC_{max}-PC_{min}) with wavelength dependence for pristine and 8% Co doped TiO_2 thin films.

pristine TiO_2 film is band to band (O_{2p}-Ti_{3d}) transition whereas small red shift can be explained on the basis of *sp-d* exchange interactions between band electrons and localized *d* electrons of cobalt ions replacing Ti ions. The *s-p* and *p-d* exchange interactions result in downward shifting of conduction band edge and upward shifting in valence band edge leading to band gap narrowing [45]. The optical band gap energy could be easily calculated from the Tauc's relation. Accordingly, Fig. 7(b) shows the plots between $(\alpha h\nu)^2$ versus photon energy ($h\nu$) to calculate band gap for all the prepared films. An extrapolation of the linear region of $(\alpha h\nu)^2$ versus $h\nu$ plot to the *x*-axis gives the value of optical band gap (E_g). The calculated values of band gap are 3.30 eV, 3.21 eV, 3.15 eV, 2.99 eV and 2.87 eV for the pristine and 2%, 4%, 6%, 8% Co doped anatase phase TiO_2 films, respectively. The band gap variation from 3.30 to 2.87 eV indicates an alteration of the electronic structure of the system. Doping of cobalt into TiO_2 may create defect levels in the band gap of TiO_2 for electron hole pair recombination at lower energy. The origin of such defect levels may be the Co itself or possibly the oxygen vacancies induced by the doping.

3.4. Photocatalytic activity

The photocatalytic activity of pristine and Co (2%, 4%, 6% and 8%) doped TiO_2 films was investigated by the degradation of two different organic dyes namely, methylene blue (MB) and azo dye as an exemplary pollutant under illumination of visible light. MB and Azo dyes are typical organic pollutants mostly coming from industrial waste and are resistant to light. However, in the presence of a photocatalytic TiO_2 surface, illumination will result in the degradation of the dye. Separate solutions of MB dye and Azo dye were prepared in deionized water and stirred in the dark for 30 min to obtain adsorption equilibrium before illumination. A visible light source was illuminated on the sample for photocatalysis, and the concentrations of the dyes were monitored by absorption spectroscopy using a UV–visible spectrophotometer. Fig. 8(a,b) shows the intensity of the absorption peak of MB (λ = 664 nm) and Azo (λ = 550 nm) dyes as a function of illumination time for the pristine and Co doped TiO_2 films as well as substrate $LaAlO_3$(100) as control sample. Fig. 8(c,d) shows the complete absorption spectrum after 70 min of illumination for each sample. The $LaAlO_3$(100) control sample was analysed to characterize the self-degradation and importance of catalyst in the degradation of dyes under the same condition. A very small degradation was observed in the presence of bare substrate $LaAlO_3$(100) which is due to adsorption of dyes on the surface of the substrate. The change in concentration observed in pristine TiO_2 thin film is because dye sensitization has played a role in degradation, having large band gap energy of TiO_2 which requires UV light to excite its electrons. Therefore, for promising results

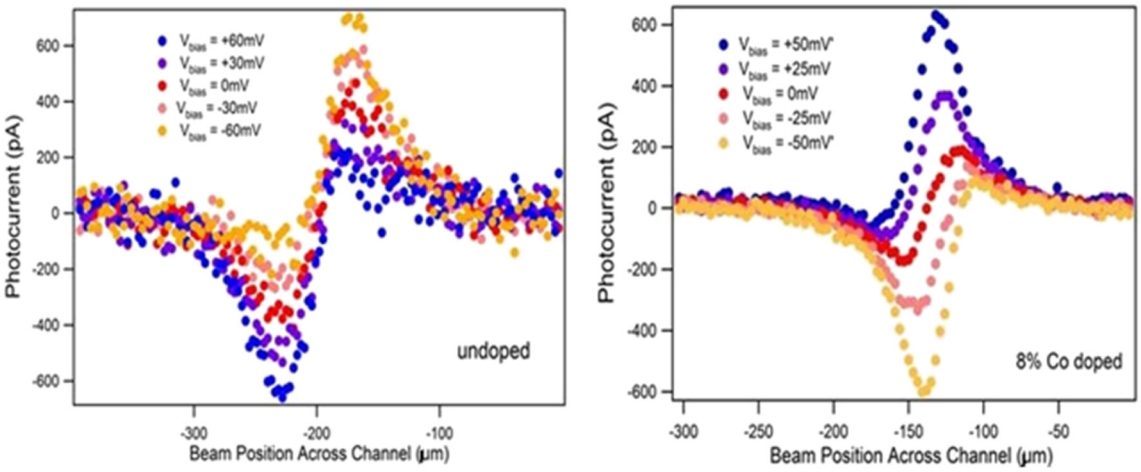

Fig. 14. Photocurrent versus beam position for pristine and 8%Co doped TiO_2 films grown on $LaAlO_3$ (100) substrate.

we need a suitable light source and catalyst for the effective degradation of dyes with time, as observed and analysed from the above experiment. The results of Fig. 8 predict that the Co doped TiO_2 films have better photocatalytic activity as the Co doping is increased for both the MB and Azo dyes. The improved photocatalytic activity with Co doping can be attributed to the red shift in optical absorption of the catalyst near visible region while pristine TiO_2 absorbs radiation below 400 nm. In our experiment, we have observed promising results, i.e. 91% degradation of MB dye and 88% degradation of Azo dye in 70 min for the 8% Co doped TiO_2 sample. This phenomenon can be explained on the basis of formation of abundant oxygen vacancies and surface defects with Co doping. However, doping has enhanced electron trapping and electron hole separation (slow electron hole recombination) as evident from the magnetic studies as well. Cheng et al. [46] have reported that the anatase Gd doped TiO_2 films have higher photocatalytic activity as compared to rutile phase TiO_2. Earlier, Fatemeh et al. [47] have also reported that TiO_2 has shown excellent photodegradation of methyl orange under visible and ultraviolet light illumination. In our results, we have also observed that as doping percentage of cobalt increases, the degradation of dyes also increases as shown in Fig. 9(a,b) indicating better photocatalytic performance. Similarly, Sonawane et al. [48] have also reported 2.5 times higher photocatalytic activity of Fe doped TiO_2 thin films than undoped film. The mechanism behind this is that the surface adsorbed dye molecules which could excite electrons and transfer them to conduction band of TiO_2 then further participate in converting into reactive oxygen species. The high degradation efficiencies of Co doped TiO_2 are attributed to the presence of negative charge on the surface of the film. A cationic MB dye can be adsorbed on the surface having highly negative charge on doped TiO_2 through the electrostatic attraction that plays an important role for the enhancement of adsorptive property and hence improve the degradation efficiency [49]. A possible photocatalytic mechanism is also shown in Fig. 9(c).

3.5. Photoconductivity

Photoconductivity is an optical and electrical phenomenon in semiconductors in which electrical conductivity is measured due to the absorption of electromagnetic radiations. There are several mechanisms involved in photoconductivity such as absorption of incident radiation, generation of electron-hole pairs, and charge carrier transport. For the excitation, the incident light must have photon energy above the band gap. The sample consists of Co-doped TiO_2 film with two Cr/Au electrodes separated by a 10 μm gap. Fig. 10 shows a scanning photocurrent map for a sample with 8% Co doping using laser wavelength of 570 nm. Fig. 11 shows detailed line cuts of the photoconductivity as a function of position for four different wavelengths. The maximum photocurrent is obtained at 480 nm wavelength and it decreases for the higher wavelength region. The decrease in photocurrent at the higher wavelength may be due to decrease in excitations of charge carriers that is attributed to the reduction in conduction current. In our study, we have compared the highest doping i.e., 8% cobalt doped TiO_2 results with the pristine TiO_2 film and shown in Fig. 12 that gives the current variation with the bias voltage. It is observed that the current for TiO_2 film is greater than cobalt doped TiO_2 due to the presence of 2 kΩ channel resistance for the doped film as compared to 1.2 kΩ channel resistance of pristine TiO_2 film. These results indicate the increase in resistance with the doping of Co ions in TiO_2 host matrix. Fig. 13 shows the PC line cut magnitude with wavelength dependence indicating almost constant behaviour at the higher wavelength and doping affect the photocurrent. By supplying the bias voltage to the photoconductor, the current flowing in the device can be obtained in the darkness and under illumination to obtain photocurrent from the system. Fig. 14 exhibits the photocurrent bias dependence behaviour that revealed opposite nature of both the samples. This opposite photocurrent direction at the metal/Schottky junction indicates different doping level between these two films. Further, on cobalt doping, the photocurrent decreases as the number density of Ti-Co nearest neighbour decreases due to the presence of impurities or oxygen vacancies that reduces the intensity of Co-Ti transition and therefore, electron hole pair density also reduces. Simultaneously, cobalt incorporation reduces band gap which splits into sets of localized Co states, that requires sufficient photoenergies for electron transfer to create electron hole pairs and transfer excited electrons from one level to another. This is consistent with the observed trend of the photocurrent. Hence the studied material is photosensitive and can be used for the solar cell applications.

4. Conclusions

In this work, we have successfully grown the anatase phase pristine and (2%, 4%, 6% and 8%) Co doped TiO_2 films onto $LaAlO_3$(100) substrate of thickness 20 nm by MBE technique. The single crystalline phase of TiO_2 and surface structural transformation have been monitored by in situ RHEED. AFM images have been analysed to confirm the surface morphology and roughness of the films. The presence of Ti^{4+}, Co^{2+} and oxygen vacancies confirmed the oxidation state of the constituent elements from XPS analysis that is used to explain observed magnetic ordering with doping. Enhancement in room temperature ferromagnetism has been observed in the prepared films and explained on the basis of oxygen vacancies created by the incorporation of cobalt in TiO_2 crystal lattice. Effect of band gap tuning was observed in TiO_2 films with the incorporation of cobalt. A red shift in the absorption

spectra is noticed that demonstrates excellent photocatalytic performance of the doped films for the degradation of MB and Azo dyes. In addition, photoconductivity was studied for the pristine and 8% cobalt doped TiO_2 films to compare the photosensitivity of the prepared films. Therefore, it is concluded that the doping of cobalt in TiO_2 matrix can alter the surface morphologies, optical and magnetic properties that may be further tuned as per applicability by varying the growth conditions for the opto-magnetic properties like photoconductivity, room temperature ferromagnetism and for waste water treatment.

Acknowledgements

One of the authors, Swaleha Naseem is highly indebted to University Grants Commission, India for providing Maulana Azad National Fellowship (MANF) (F117.1/201415/MANF-201415-MUS-UTT-33700/(SAIII/Website)) and United States India Education Foundation (USIEF) for providing Indo-US STEM ER fellowship under OSU-AMU collaboration. Special thanks to Physics Research department, The Ohio State University (OSU), U.S.A for providing experimental facilities. Prof. Chang-Mou Wu, National Taiwan University of Science and Technology, Taipei is thanked for his help in XPS measurements.

References

[1] T. Dietl, Spintronics and ferromagnetism in wide-band-gap semiconductors, AIP Conf. Proc. 772 (2005) 56–64, https://doi.org/10.1063/1.1993996.
[2] X.Y. Li, S.X. Wu, L.M. Xu, C.T. Li, Y.J. Liu, X.J. Xing, et al., Effects of depositing rate on structure and magnetic properties of Mn:TiO_2 films grown by plasma-assisted molecular beam epitaxy, Mater. Sci. Eng. B Solid-State Mater. Adv. Technol. 156 (2009) 90–93, https://doi.org/10.1016/j.mseb.2008.11.036.
[3] S.A. Chambers, Ferromagnetism in doped thin-film oxide and nitride semiconductors and dielectrics, Surf. Sci. Rep. 61 (2006) 345–381, https://doi.org/10.1016/j.surfrep.2006.05.001.
[4] Z.Y. Wu, F.R. Chen, J.J. Kai, W.B. Jian, J.J. Lin, Fabrication, characterization and studies of annealing effects on ferromagnetism in $Zn_{1-x}Co_xO$ nanowires, Nanotechnology 17 (2006) 5511–5518, https://doi.org/10.1088/0957-4484/17/21/036.
[5] S. Naseem, W. Khan, S. Khan, S. Husain, A. Ahmad, Dielectric response and room temperature ferromagnetism in Cr doped anatase TiO_2 nanoparticles, J. Magn. Magn. Mater. 447 (2018) 155–166, https://doi.org/10.1016/j.jmmm.2017.09.051.
[6] Y. Matsumoto, Room-temperature ferromagnetism in transparent transition metal-doped titanium dioxide, Science (80-) 291 (2001) 854–856, https://doi.org/10.1126/science.1056186.
[7] T. Dietl, H. Ohno, F. Matsukura, J. Cibert, D. Ferrand, Zener model description of ferromagnetism in zinc-blende magnetic semiconductors, Science (80-.) 287 (2000) 1019–1022, https://doi.org/10.1126/science.287.5455.1019.
[8] K. Yang, R. Wu, L. Shen, Y.P. Feng, Y. Dai, B. Huang, Origin of d^0 magnetism in II-VI and III-V semiconductors by substitutional doping at anion site, Phys. Rev. B - Condens. Matter Mater. Phys. 81 (2010) 1–5, https://doi.org/10.1103/PhysRevB.81.125211.
[9] J.M.D. Coey, M. Venkatesan, C.B. Fitzgerald, Donor impurity band exchange in dilute ferromagnetic oxides, Nat. Mater. 4 (2005) 173–179, https://doi.org/10.1038/nmat1310.
[10] P.M. Perillo, D.F. Rodríguez, Low temperature trimethylamine flexible gas sensor based on TiO_2 membrane nanotubes, J. Alloys Compd. 657 (2016) 765–769, https://doi.org/10.1016/j.jallcom.2015.10.167.
[11] M. Paulose, K. Shankar, O.K. Varghese, G.K. Mor, C.A. Grimes, Application of highly-ordered TiO_2 nanotube-arrays in heterojunction dye-sensitized solar cells, J. Phys. D. Appl. Phys. 39 (2006) 2498–2503, https://doi.org/10.1088/0022-3727/39/12/005.
[12] X. Lü, X. Mou, J. Wu, D. Zhang, L. Zhang, F. Huang, et al., Improved-performance dye-sensitized solar cells using Nb-doped TiO_2 electrodes: efficient electron injection and transfer, Adv. Funct. Mater. 20 (2010) 509–515, https://doi.org/10.1002/adfm.200901292.
[13] A. Fujishima, 1972 Nature Publishing Group, Nature. 238 (1972) 37–38. doi:org/https://doi.org/10.1038/238037a0.
[14] A. Sclafani, J.M. Herrmann, Comparison of the photoelectronic and photocatalytic activities of various anatase and rutile forms of titania in pure liquid organic phases and in aqueous solutions, J. Phys. Chem. 100 (1996) 13655–13661.
[15] J. Zhu, F. Chen, J. Zhang, H. Chen, M. Anpo, Fe^{3+}-TiO_2 photocatalysts prepared by combining sol-gel method with hydrothermal treatment and their characterization, J. Photochem. Photobiol. A Chem. 180 (2006) 196–204, https://doi.org/10.1016/j.jphotochem.2005.10.017.
[16] R. Asahi, Visible-light photocatalysis in nitrogen-doped titanium oxides, Science (80-.) 293 (2001) 269–271, https://doi.org/10.1126/science.1061051.
[17] H. Lin, C. Shih, Efficient one-pot microwave-assisted hydrothermal synthesis of M (M = Cr, Ni, Cu, Nb) and nitrogen co-doped TiO_2 for hydrogen production by photocatalytic water splitting, J. Mol. Catal. A Chem. 411 (2016) 128–137.
[18] O. Carp, C.L. Huisman, A. Reller, Photoinduced reactivity of titanium dioxide, Prog. Solid State Chem. 32 (2004) 33–177, https://doi.org/10.1016/j.progsolidstchem.2004.08.001.
[19] K. Pomoni, A. Vomvas, C. Trapalis, Electrical conductivity and photoconductivity studies of TiO_2 sol-gel thin films and the effect of N-doping, J. Non-Cryst. Solids 354 (2008) 4448–4457, https://doi.org/10.1016/j.jnoncrysol.2008.06.069.
[20] N. Serpone, D. Lawless, J. Disdier, J.M. Herrmann, Spectroscopic, photoconductivity, and photocatalytic studies of TiO_2 colloids: naked and with the lattice doped with Cr^{3+}, Fe^{3+}, and V^{5+} cations, Langmuir 10 (1994) 643–652, https://doi.org/10.1021/la00015a010.
[21] S. Kitazawa, S. Yamamoto, Preparation of functional TIO 2 films by pulsed laser, Adv. Chem. Res. 4 (2015) 56–106.
[22] R. Shao, C. Wang, D.E. McCready, T.C. Droubay, S.A. Chambers, Growth and structure of MBE grown TiO_2 anatase films with rutile nano-crystallites, Surf. Sci. 601 (2007) 1582–1589, https://doi.org/10.1016/j.susc.2007.01.039.
[23] S.A. Chambers, S. Thevuthasan, R.F.C. Farrow, R.F. Marks, J.U. Thiele, L. Folks, et al., Epitaxial growth and properties of ferromagnetic co-doped TiO_2 anatase, Appl. Phys. Lett. 79 (2001) 3467–3469, https://doi.org/10.1063/1.1420434.
[24] N.V. Burbure, P.A. Salvador, G.S. Rohrer, Influence of dipolar fields on the photochemical reactivity of thin titania films on $BaTiO_3$ substrates, J. Am. Ceram. Soc. 89 (2006) 2943–2945, https://doi.org/10.1111/j.1551-2916.2006.01168.x.
[25] P.J. Hansen, V. Vaithyanathan, Y. Wu, T. Mates, S. Heikman, U.K. Mishra, et al., Rutile films grown by molecular beam epitaxy on GaN and AlGaN/GaN, J. Vac. Sci. Technol. B Microelectron. Nanom. Struct. 23 (2005) 499, https://doi.org/10.1116/1.1868672.
[26] P. Fisher, O. Maksimov, H. Du, V.D. Heydemann, M. Skowronski, P.A. Salvador, Growth, structure, and morphology of TiO_2 films deposited by molecular beam epitaxy in pure ozone ambients, Microelectron. J. 37 (2006) 1493–1497, https://doi.org/10.1016/j.mejo.2006.05.010.
[27] S.A. Chambers, C.M. Wang, S. Thevuthasan, T. Droubay, D.E. Mccready, A.S. Lea, et al., Epitaxial growth and properties of MBE-grown ferromagnetic Co-doped TiO 2 anatase films on $SrTiO_3$ (001) and $LaAlO_3$ (001), Thin Solid Films 418 (2002) 197–210.
[28] L.M. Xu, M. Yang, X.Y. Li, P. Hu, S.W. Li, Effect of growth temperature on ferromagnetism in Mn:TiO_2 thin film grown on $SrTiO_3$:Nb substrate, Scr. Mater. 63 (2010) 113–116, https://doi.org/10.1016/j.scriptamat.2010.03.027.
[29] H.H. Nguyen, J. Sakai, W. Prellier, A. Hassini, A. Ruyter, F. Gervais, Ferromagnetism in transition-metal-doped TiO_2 thin films, Phys. Rev. B - Condens. Matter Mater. Phys. 70 (2004) 1–6, https://doi.org/10.1103/PhysRevB.70.195204.
[30] J.F. Moulder, W.F. Stickle, P.E. Sobol, K.D. Bomben, Handbook of X-ray Photoelectron Spectroscopy, (1992), https://doi.org/10.1002/sia.740030412.
[31] S. Naseem, W. Khan, S. Khan, S. Husain, A. Ahmad, Consequences of (Cr/Co) co-doping on the microstructure, optical and magnetic properties of microwave assisted sol-gel derived TiO_2 nanoparticles, J. Lumin. 205 (2019) 406–416, https://doi.org/10.1016/j.jlumin.2018.09.022.
[32] V.R. Akshay, B. Arun, G. Mandal, A. Chanda, M. Vasundhara, Significant reduction in the optical band-gap and defect assisted magnetic response in Fe-doped anatase TiO_2 nanocrystals as dilute magnetic semiconductors, New J. Chem. 43 (2019) 6048–6062, https://doi.org/10.1039/c9nj00275h.
[33] B. Bharti, S. Kumar, H.-N. Lee, R. Kumar, Formation of oxygen vacancies and Ti^{3+} state in TiO_2 thin film and enhanced optical properties by air plasma treatment, Sci. Rep. 6 (2016) 32355, , https://doi.org/10.1038/srep32355.
[34] B. Choudhury, A. Choudhury, A.K.M. Maidul Islam, P. Alagarsamy, M. Mukherjee, Effect of oxygen vacancy and dopant concentration on the magnetic properties of high spin Co^{2+} doped TiO_2 nanoparticles, J. Magn. Magn. Mater. (2011), https://doi.org/10.1016/j.jmmm.2010.09.043.
[35] Y. Bai, J. Chen, S. Zhao, Q. Lu, Magneto-dielectric and magnetoelectric anisotropies of $CoFe_2O_4/Bi_5Ti_3FeO_{15}$ bilayer composite heterostructural films, RSC Adv. 6 (2016) 52353–52359, https://doi.org/10.1039/C6RA07933D.
[36] S. Kumar, M. Srivastava, J. Singh, S. Layek, M. Yashpal, A. Materny, et al., Controlled synthesis and magnetic properties of monodispersed ceria nanoparticles controlled synthesis and magnetic properties of monodispersed ceria nanoparticles, AIP Adv. 5 (2015) 27109, https://doi.org/10.1063/1.4908003.
[37] N.H. Hong, J. Sakai, N. Poirot, V. Brizé, Room-temperature ferromagnetism observed in undoped semiconducting and insulating oxide thin films, Phys. Rev. B - Condens. Matter Mater. Phys. 73 (2006) 3–6, https://doi.org/10.1103/PhysRevB.73.132404.
[38] K.J. Kim, Y. Ran Park, J. Han Lee, S.L. Choi, H. Jung Lee, C. Sung Kim, et al., Room-temperature ferromagnetic properties in Mn-doped rutile TiO_2 thin films, J. Magn. Magn. Mater. 316 (2007) 215–218, https://doi.org/10.1016/j.jmmm.2007.02.093.
[39] S.K.S. Patel, N.S. Gajbhiye, Oxygen deficiency induced ferromagnetism in Cr-doped TiO_2 nanorods, J. Magn. Magn. Mater. 330 (2013) 21–24, https://doi.org/10.1016/j.jmmm.2012.09.043.
[40] D.A. Schwanz, D.R. Gamelin, Reversible 300 K ferromagnetic ordering in a diluted magnetic semiconductor, Adv. Mater. 16 (2004) 2115–2119, https://doi.org/10.1002/adma.200400456.
[41] J.M. Coey, M. Venkatesan, C.B. Fitzgerald, Donor impurity band exchange in dilute ferromagnetic oxides, Nat. Mater. 4 (2005) 173–179, https://doi.org/10.1038/nmat1310.
[42] L.M. Xu, Y.P. Yu, X.J. Xing, X.Y. Wu, S.W. Li, Enhancement of ferromagnetism upon thermal annealing in plasma assisted MBE grown mixed-phase Mn-doped insulating TiO_2 thin films, Appl. Phys. A Mater. Sci. Process. 92 (2008) 361–365, https://doi.org/10.1007/s00339-008-4530-2.
[43] A. Kaminski, S. Das Sarma, Polaron percolation in diluted magnetic semiconductors, Phys. Rev. Lett. 88 (2002) 247202, , https://doi.org/10.1103/

PhysRevLett.88.247202.
[44] L. Samet, J. Ben Nasseur, R. Chtourou, K. March, O. Stephan, Heat treatment effect on the physical properties of cobalt doped TiO_2 sol-gel materials, Mater. Charact. 85 (2013) 1–12, https://doi.org/10.1016/j.matchar.2013.08.007.
[45] B. Santara, B. Pal, P.K. Giri, Signature of strong ferromagnetism and optical properties of Co doped TiO 2 nanoparticles, J. Appl. Phys. 110 (2011) 114322, , https://doi.org/10.1063/1.3665883.
[46] X.Q. Cheng, C.Y. Ma, X.Y. Yi, F. Yuan, Y. Xie, J.M. Hu, et al., Structural, morphological, optical and photocatalytic properties of Gd-doped TiO_2 films, Thin Solid Films 615 (2016) 13–18, https://doi.org/10.1016/j.tsf.2016.06.049.
[47] F. Mostaghni, Y. Abed, Structural, optical and photocatalytic properties of Co-TiO_2 prepared by sol-gel technique, Mater. Res. 19 (2016) 741–745, https://doi.org/10.1590/1980-5373-MR-2016-0191.
[48] R.S. Sonawane, B.B. Kale, M.K. Dongare, Preparation and photo-catalytic activity of Fe-TiO_2 thin films prepared by sol-gel dip coating, Mater. Chem. Phys. 85 (2004) 52–57, https://doi.org/10.1016/j.matchemphys.2003.12.007.
[49] F. Azeez, E. Al-hetlani, M. Arafa, Y. Abdelmonem, A.A. Nazeer, M.O. Amin, et al., The effect of surface charge on photocatalytic degradation of methylene blue dye using chargeable titania nanoparticles, Sci. Rep. 8 (2018) 7104, , https://doi.org/10.1038/s41598-018-25673-5.